SANDIA REPORT
SAND2012-4646
Unlimited Release
Printed June 2012

Optical Spectroscopy Results for the Self-Magnetic Pinch Electron Beam Diode on the RITS-6 Accelerator

Mark D. Johnston, Bryan V. Oliver, Kelly Hahn, Darryl W. Droemer, Marlon D. Crain, Dale R. Welch, Yitzhak Maron

Prepared by
Sandia National Laboratories
Albuquerque, New Mexico 87185 and Livermore, California 94550

Sandia National Laboratories is a multi-program laboratory managed and operated by Sandia Corporation, a wholly owned subsidiary of Lockheed Martin Corporation, for the U.S. Department of Energy's National Nuclear Security Administration under contract DE-AC04-94AL85000.

Issued by Sandia National Laboratories, operated for the United States Department of Energy by Sandia Corporation.

Available to DOE and DOE contractors from
U.S. Department of Energy
Office of Scientific and Technical Information
P.O. Box 62
Oak Ridge, TN 37831

Telephone: (865) 576-8401
Facsimile: (865) 576-5728
E-Mail: reports@adonis.osti.gov
Online ordering: http://www.osti.gov/bridge

Available to the public from
U.S. Department of Commerce
National Technical Information Service
5285 Port Royal Rd.
Springfield, VA 22161

Telephone: (800) 553-6847
Facsimile: (703) 605-6900
E-Mail: orders@ntis.fedworld.gov
Online order: http://www.ntis.gov/help/ordermethods.asp?loc=7-4-0#online

SAND2012-4646
Unlimited Release
Printed June 2012

Optical Spectroscopy Results for the Self-Magnetic Pinch Electron Beam Diode on the RITS-6 Accelerator

Mark D. Johnston, Bryan V. Oliver, and Kelly Hahn
Advanced Radiographic Technologies Department
Sandia National Laboratories
P.O. Box 5800
Albuquerque, New Mexico 87185-MS1168

Darryl W. Droemer and Marlon D. Crain
National Security Technologies, LLC
P.O. Box 98521
Las Vegas, NV 89193

Dale R. Welch
Voss Scientific, LLC, 418 Washington St.
Albuquerque, NM 87108

Yitzhak Maron
Weizmann Institute of Science
Rehovot, Israel 76100

Abstract

Experiments have been conducted at Sandia National Laboratories' RITS-6 accelerator facility [1] (operating at 7.5 MV and 180 kA) investigating plasma formation and propagation in relativistic electron beam diodes used for flash x-ray radiography. High resolution, visible and ultraviolet spectra were collected in the anode-cathode (A-K) vacuum gap of the Self-Magnetic Pinch (SMP) diode [2-4]. Time and space resolved spectra are compared with time-dependent, collisional-radiative (CR) calculations [5-7] and Lsp, hybrid particle-in-cell code simulations [8,9]. Results indicate the presence of a dense ($>1x10^{17}cm^{-3}$), low temperature (few eV), on-axis plasma, composed of hydrocarbon and metal ion species, which expands at a rate of several cm/μs from the anode to the cathode. In addition, cathode plasmas are observed which extend several millimeters into the A-K gap [10]. It is believed that the interaction of these electrode plasmas cause premature impedance collapse of the diode and subsequent reduction in the total radiation output. Diagnostics include high speed imaging and spectroscopy using nanosecond gated ICCD cameras, streak cameras, and photodiode arrays.

ACKNOWLEDGMENTS

Sandia National Laboratories is a multi-program laboratory managed and operated by Sandia Corporation, a wholly owned subsidiary of Lockheed Martin Corporation, for the U.S. Department of Energy's National Nuclear Security Administration under contract DE-AC04-94AL85000.

CONTENTS

FIGURES

1. INTRODUCTION

A series of self-magnetic pinch diode shots were taken on the RITS-6 (7.5 MV, 180 kA) accelerator [1] during which optical spectroscopy diagnostics were fielded. These diagnostics were fielded to gain a better understanding of plasma formation and propagation in vacuum diodes and their effects on diode performance. The SMP diode (figure 1) consists of a hollow, aluminum cathode and a thin aluminum foil anode. Behind the aluminum foil is positioned a ~1/3 electron range tantalum target used to generate bremsstrahlung x-rays. Electrons accelerated across a short, centimeter wide vacuum gap, are focused to a few millimeters diameter at the target, generating very high MA/cm^2 current densities. As the electrons impinge on the anode, plasma ion species are evolved which can accelerate back across the A-K gap and cause premature impedance collapse of the diode. Details regarding the operation and performance of this diode, and in particular, the geometry associated with its operation on RITS when configured with a low (40 Ohms) impedance MITL have been reported [2]. The results presented here are the first direct spectroscopic measurements of the plasma processes that occur within the diode.

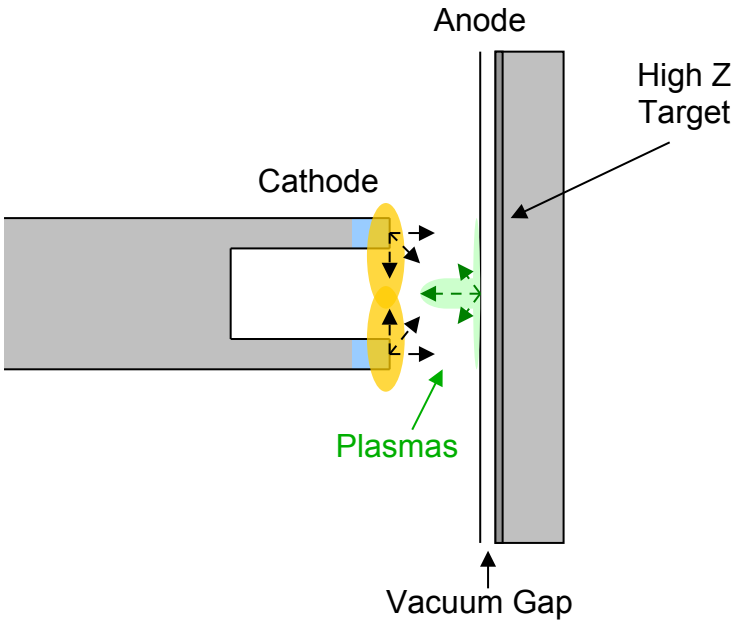

Figure 1. Self-Magnetic Pinch Diode Configuration.

Pinch beam diodes have been studied and used as bremsstrahlung x-ray sources for many years [11-14]. It is well established that ion formation on the anode surface, due to heating from incident electrons, is necessary for pinching the electron beam to the axis [15,16]. It is generally believed that surface contaminants such as hydrogen, carbon, and oxygen, from water vapor and hydrocarbon residues, are the main constituents of these plasmas [17]. What is less understood is the process by which these ions expand into the vacuum gap and their role in the overall impedance behavior of the diode. Similarly, the behavior of ions created within the vacuum gap by processes such as electron impact ionization and charge exchange with neutrals is not well understood. This paper offers the first experimental evidence which shows anode plasmas expanding into the A-K gap during the ~70 ns electron beam pulse.

2. Experimental Configuration: (Shots 409-416)

The diagnostics employed were streaked optical spectra, using a 1 meter McPherson monochromator (Model 2061) [18] with a 150 groove/mm diffraction grating (5000 Angstrom blaze angle) recorded on an NSTec L-CA-24 streak camera [19,20] with a 10 ns/mm sweep speed. The settings were chosen to allow maximum flexibility both in time and wavelength in the data collection. Further studies at higher spectral and temporal resolutions are planned. The spectra were collected through ten meters of 200 μm diameter optical fused silica fiber (Polymicro FVP-200) [21], at various axial locations within the A-K vacuum region, and at two radial positions (r = 0mm, and r = 7.5mm). Figure 2 shows the focusing optics used to collect light from the diode region. Spectra were collected on separate shots, with the two radii chosen to aid in determining plasma size and expansion in time.

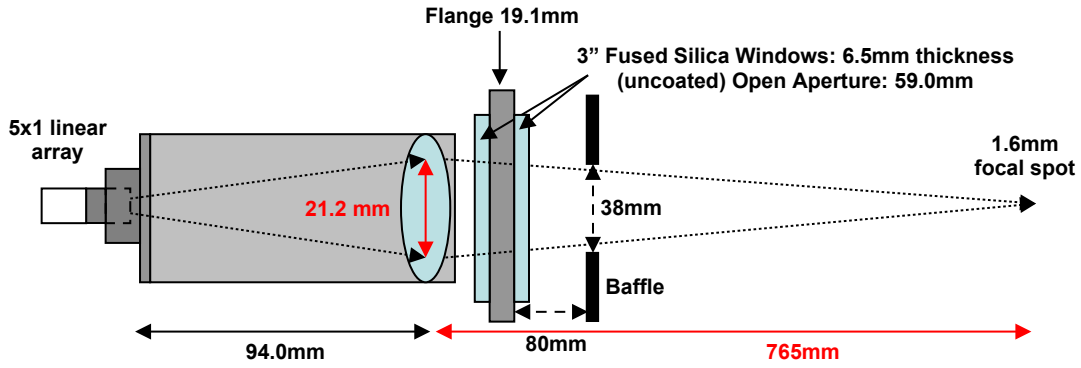

Figure 2. Light collection optics for SMP diode spectra (shots 409-416).

3. Experimental Results: (Shots 409-416)

From figure 3 we can see that visible light emission begins on-axis at the anode (green curve) and cathode (blue curve) mid-way through the radiation pulse, when the voltage is at its maximum (see figure 12). At 6.5mm off-axis (figure 4), the light emission is reduced in intensity and delayed in time (radius of the cathode is 6.25mm).

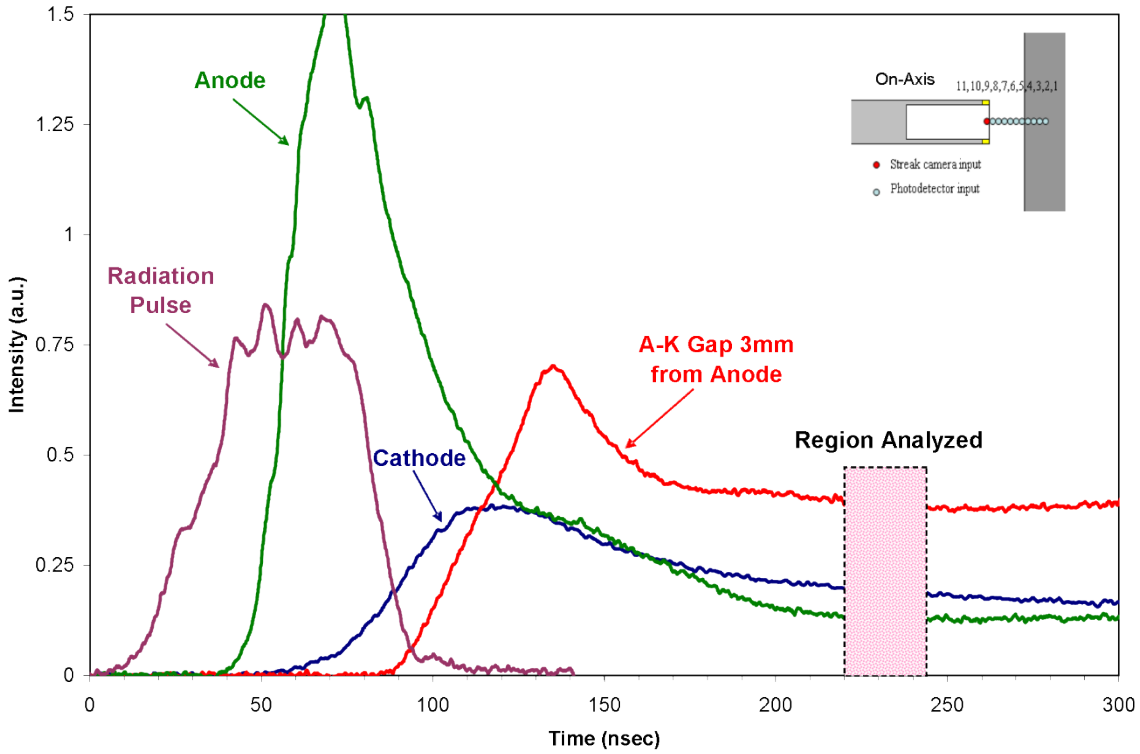

Figure 3. Visible light emission (silicon PIN photodiodes) (on-axis).

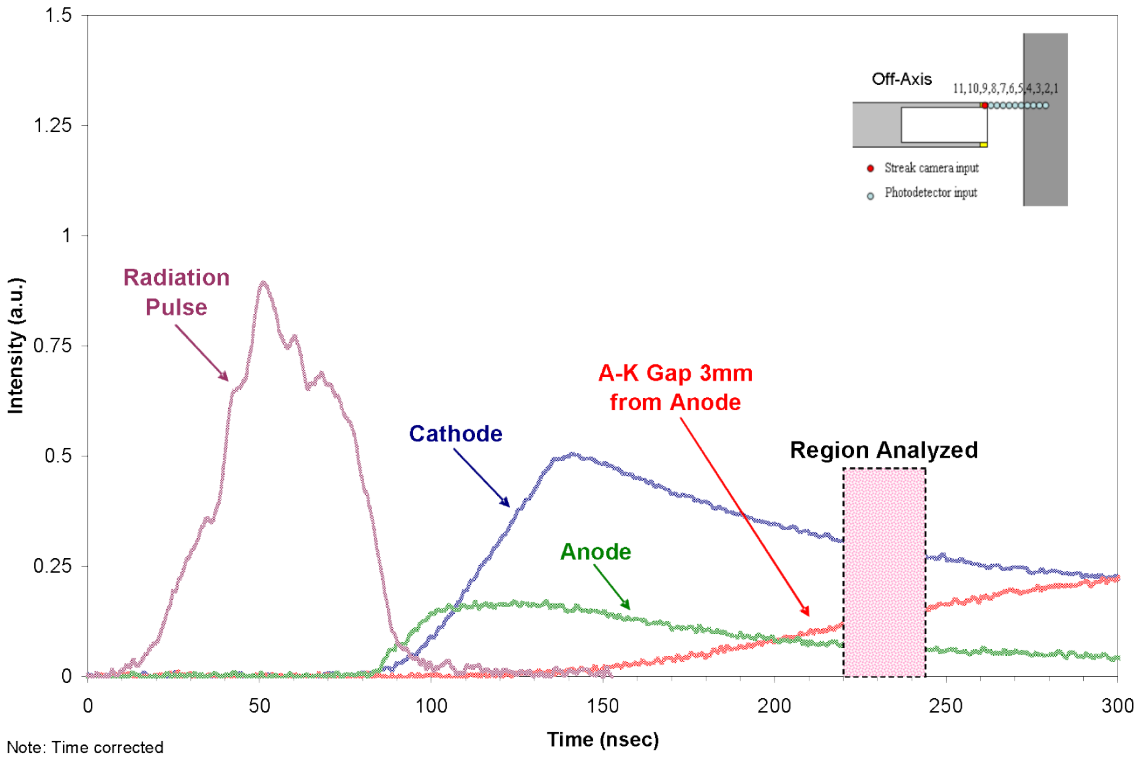

Figure 4. Visible light emission (silicon PIN photodiodes) (6.5mm off-axis).

Two sets of shots were taken on the SMP diode looking at visible/uv emission spectra in the A-K gap region. The first set (409-416) looked at emission from 3100Å to 4600Å. These measurements covered a broad spectral range (~1500Å) in the visible/uv using simple (plano-convex) fused silica optics. The fiber array and optics used for shots (409-416) had a 1.6mm focal diameter at the diode (figure 2). Chromatic aberrations were present, along with variations in the focal plane with wavelength (figure 5), which made interpretation of the data difficult [22].

90mm FL Plano-Convex Fused Silica Lens

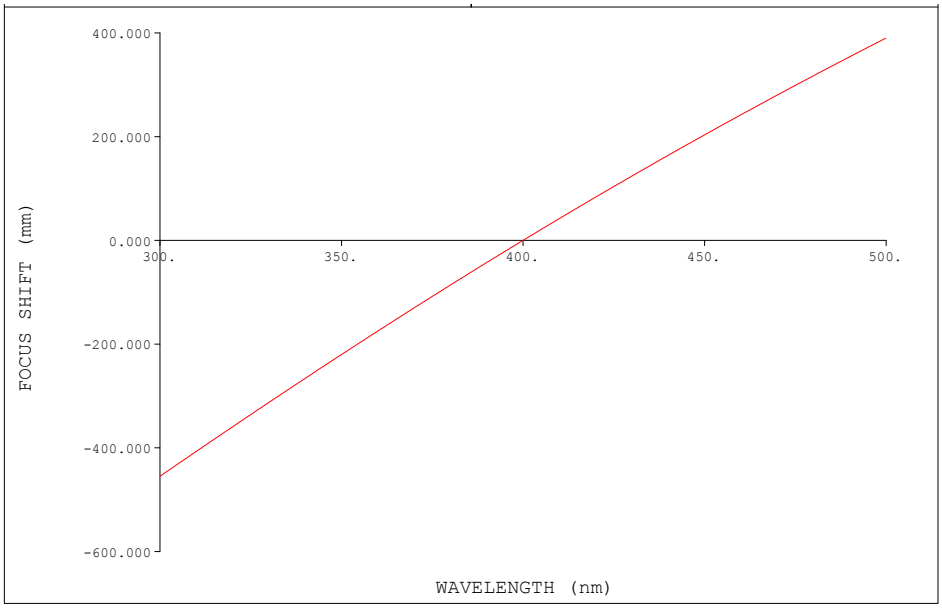

Figure 5. Focal spot versus wavelength for SMP shots 409-416.

The spectra showed large variations in intensity from the on-axis to off-axis regions (7.5 mm, just beyond the physical diameter of the cathode). Spectra were taken at several locations across the A-K gap, and two of the shots (411 and 412, taken 3 mm from the anode surface) were analyzed in detail.

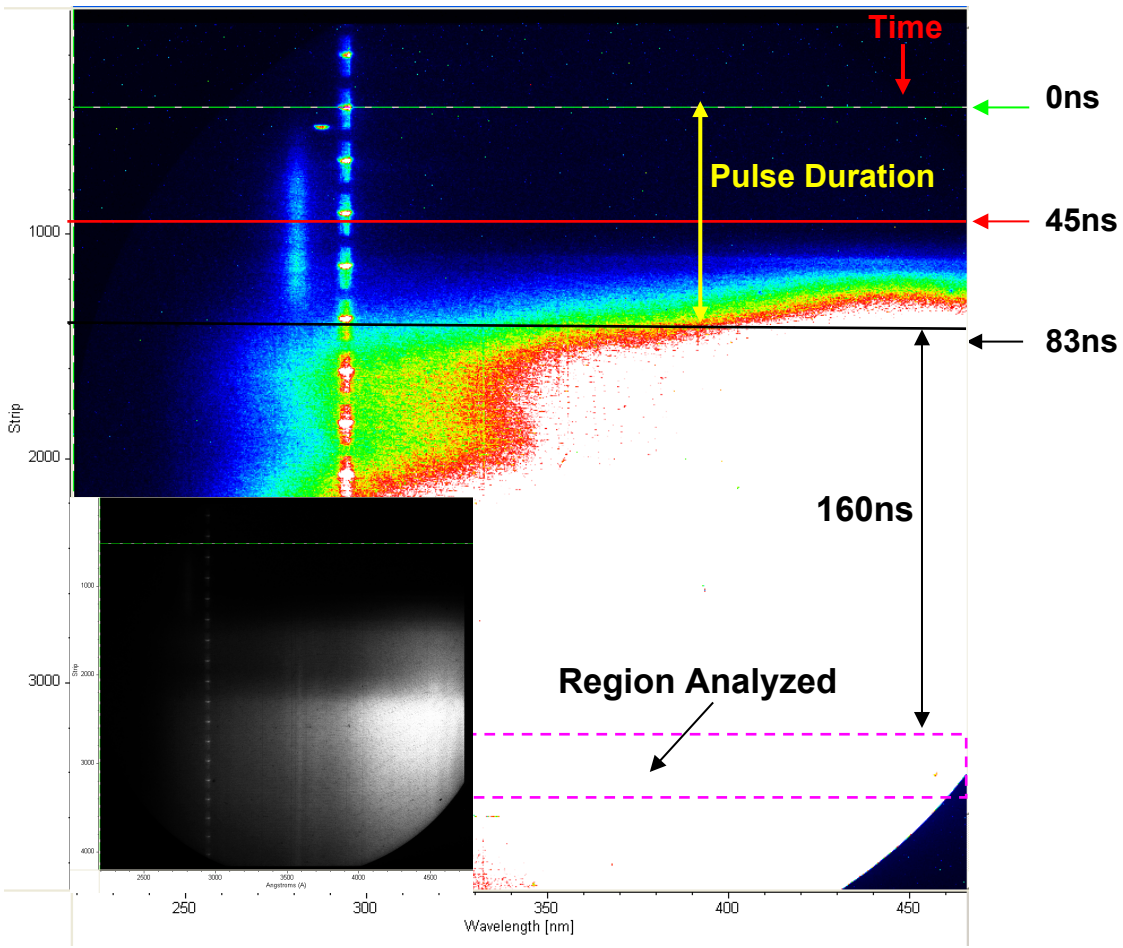

Figure 6. On-axis streak camera spectra (shot 411).

The spectra consisted of bright continuum emission on-axis with little or no line emission until late in time (the streak camera covers ~300 ns, starting when current first reaches the diode) (figure 6). Off axis, the total intensity is less and line emission is observed (figure 7); however, the off-axis spectra are delayed in time relative to the on-axis spectra due to time-of-flight for the plasma to reach that location in sufficient numbers to be measured. Assuming the plasma originates from a small region (~3 mm diameter) on the surface of the anode where the beam is focused, then by simple geometry, and the time of flight for the observed signals, the expansion velocities are ~7 cm/μsec.

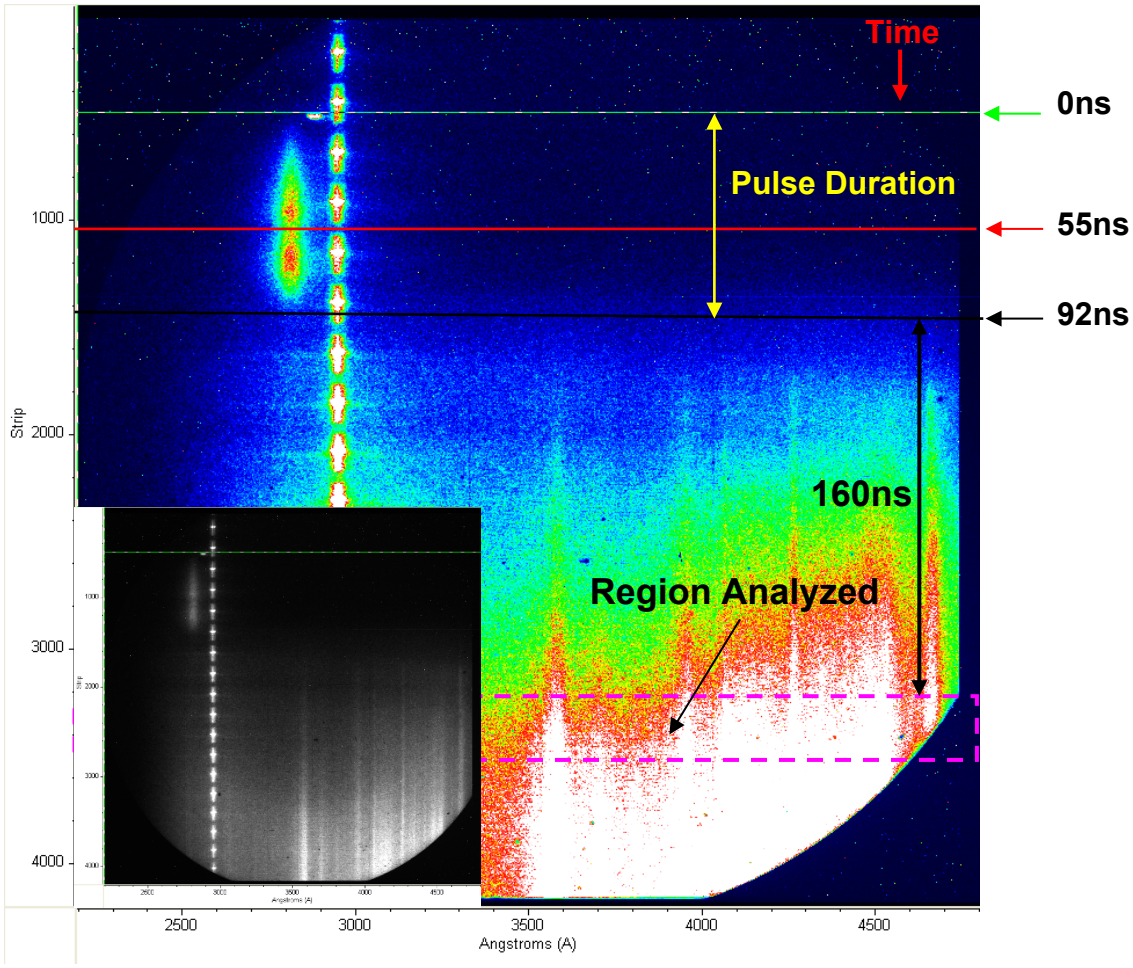

Figure 7. Off-axis streak camera spectra (shot 412).

Even considering differences in the chordal lines of sight (figure 8), it is apparent that the on-axis plasma is much brighter (denser) than the off-axis plasma. Since absolute calibrations were not performed on these shots, it was decided to calibrate the data by using the late-time spectra measured at large radii, and relating it back to the early-time on-axis continuum spectra (see "region analyzed" in figures 3,4,6, and 7) [23]. With a spectral resolution of 12 Angstroms, we observed line broadening for both aluminum and carbon lines (determined to be Stark broadening), indicating the presence of high electron densities (>10^17 cm^{-3}).

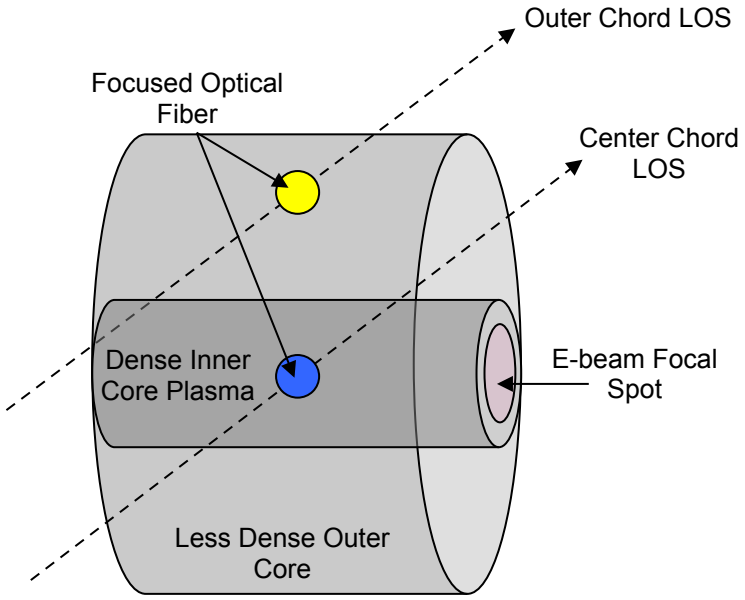

Figure 8. Chordal Lines of Sight through SMP diode plasmas.

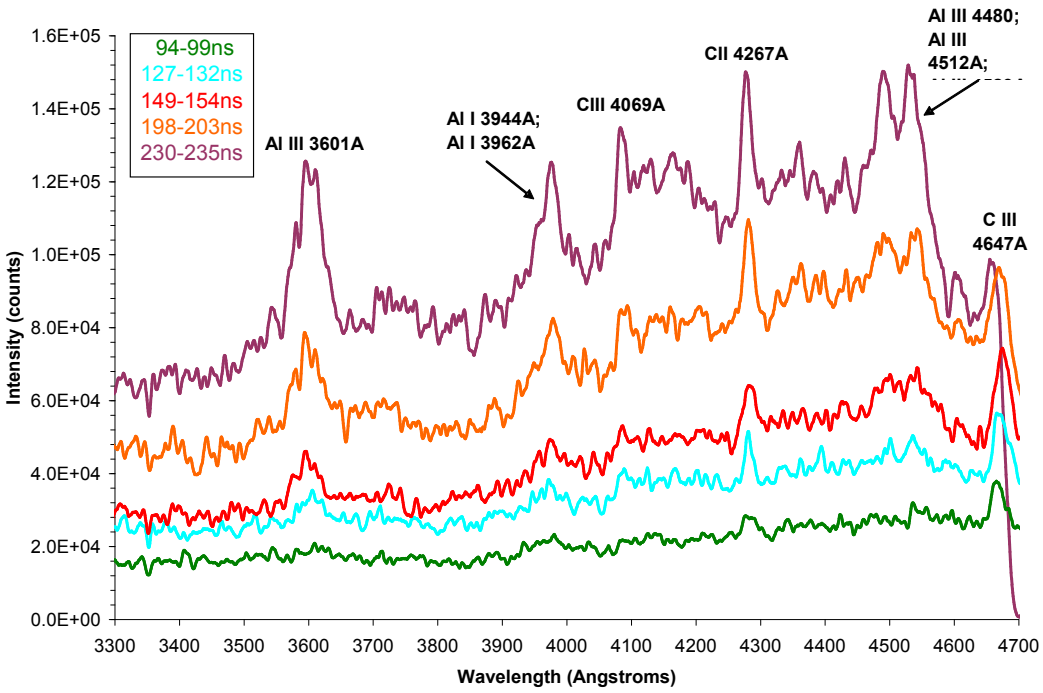

Figure 9. SMP Shot 412 (7.5mm off-axis).

Obtaining the electron densities from the linewidths (independent of pathlength through the plasma), allowed us to calibrate the continuum in terms of electron density (linewidths of 20 Angstroms were measured for the C II 4267Å line). Using this technique, the continuum late in time (235ns) for the off-axis spectra (shot 411) was determined to have an electron density (N_e) of $3x10^{18}$ cm^{-3}. Figure 10 shows a representative plot of the experimental data along with calculated spectra which considers contributions from both lines and continuum. Knowing the absolute continuum intensity, the absolute line intensities could also be determined, which allowed for ion density determinations. This technique assumes that the line and continuum emission come from the same plasma volume. From these calculations, the aluminum and carbon ion densities at 235ns were determined to be $5x10^{16}$ cm^{-3} and $1x10^{17}$ cm^{-3}, respectively, both well below the $3x10^{18}$ cm^{-3} electron density determined from the Stark-broadened linewidths. Even with multiple charge states present, this requires another source to provide the necessary electrons. One explanation is that electrons from ionized hydrogen, known to be a prevalent contaminant in pulsed-power diodes, are responsible for the high electron densities, and since ionized hydrogen (protons) has no spectral lines, this would account for the lack of line emission early-in-time. The electron temperatures obtained from relative line ratios of carbon and aluminum ion lines (a few eV) were used in the electron density determinations (see figure 10).

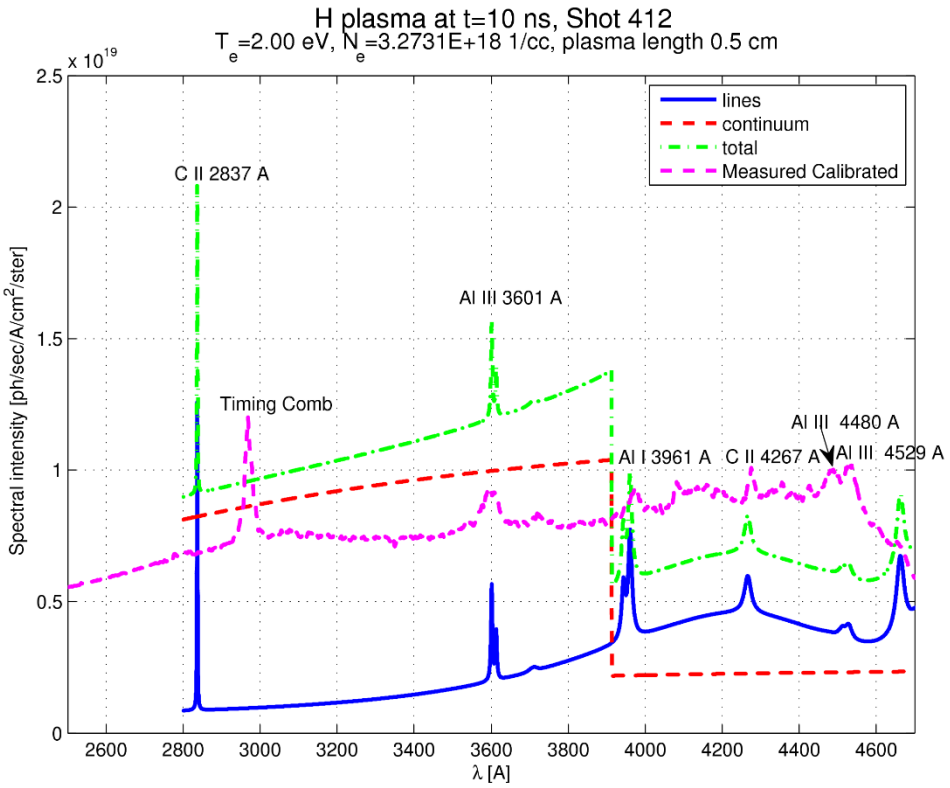

Figure 10. Experimental and Calculated Off-axis SMP spectra (non-uniformity in calculated spectra due to hydrogen Balmer series transitions).

The calibrated continuum intensities for the off-axis spectra late-in-time were related back to the on-axis spectra. While considerations were made regarding the origins of the continuum, which include free-free and free-bound electron considerations, to the first order, over small changes (few eV) in temperature, the continua can be related to each other by the square root of the intensity (assuming a uniform plasma, 5mm in length along the line of sight) [24]. The length assumption introduces some error into the calculations, since the plasma is continually expanding during this period. Using this technique, the on-axis continuum was determined to be 1x10^19 cm^{-3} at late-time (250 ns for shot 411) and 1x10^18 cm^{-3} at early time (50-55 ns) during the second half of the radiation pulse. The continua signals were first measurable above the background at about mid-pulse (~50 ns after the time when the current first reaches the diode), and during the ~30 ns from the mid-pulse to the end of the radiation pulse, the density increased linearly by a factor of 5 (figure 11). This linear increase in density mirrors the linear increase in

current flowing in the diode and the subsequent linear decrease in impedance (figure 12). A more detailed description of the continua spectra will be given in a subsequent report.

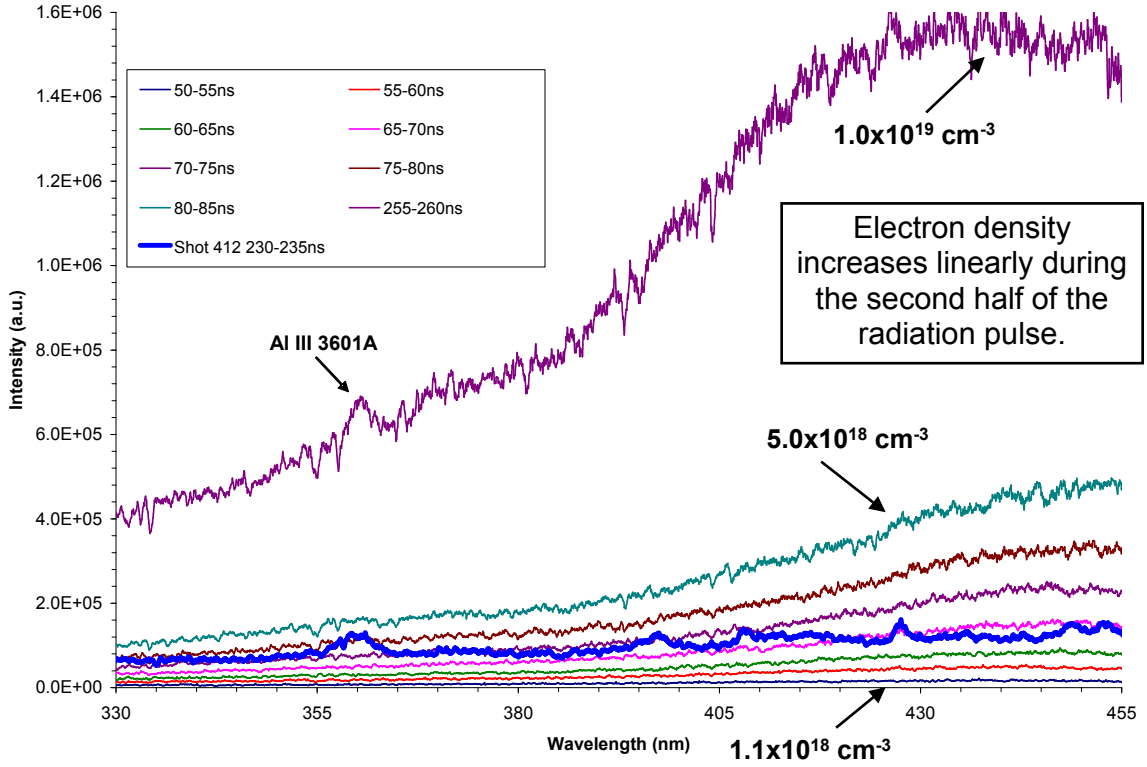

Figure 11. Electron density increase with time on-axis (shot 411) with off-axis late-time lineout from (shot 412) superimposed in blue.

4. Conclusions: (Shots 409-416)

From the CR calculations, it was concluded that at 3mm (+/- 0.1mm) from the anode surface, the electron density was $1x10^{18}$ cm^{-3} (+/- 20%) and the electron temperature was 2 eV during the radiation pulse. Since no lines were observed, and analyses of the off-axis spectra showed low concentrations of aluminum and carbon, we hypothesized that protons from hydrogen contaminants on the surface of the anode foil were responsible for the on-axis continuum. It seems reasonable that hydrogen, known to be present in vacuum diodes, easy to desorb, very light, and very fast, should be a major constituent of the early-time plasma. There is some question as to the amount of hydrogen present from water vapor and hydrocarbons (RITS is a very dirty vacuum system with a typical pressure of ~$1x10^{-5}$ Torr), but it is assumed that enough monolayers of hydrogen contaminants (upwards of 100) are present to support the measured densities [16] (see appendix).

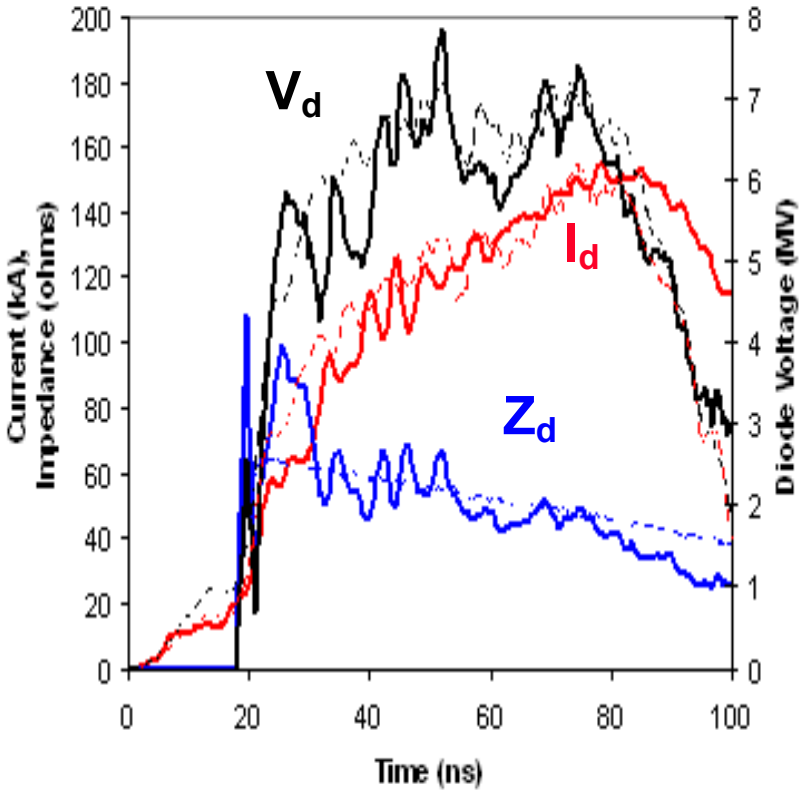

Figure 12. SMP diode current, voltage, and impedance.

SEM analyses of the aluminum foil could be conducted to better quantify the amounts of surface contaminants. In addition foil heating experiments would corroborate these results, as removal of large amounts of surface contaminants by heating would result in a subsequent decrease in the total continuum emission. On the other hand, if the continua are due to electrons from the base anode material (aluminum), then heating should have little or no effect on the measured levels.

5. Experimental Configuration: (Shots 762-767)

Having gained a lot of insight into the diode and diagnostics during the initial shot campaign (shots 409-416), it was decided to conduct another series of shots with improved diagnostics to try and expand upon the earlier results. For this series of shots (762-767), the diode configuration was identical to that of shots 409-416. For these shots, the diagnostics were improved, and we went back to the visible region where the system's collection efficiency is better. We used the same 5000Å blaze angle grating as during the previous run, and built a new 10 meter (11x1) quartz optical fiber array. In the visible, we used an achromatic lens to provide better focusing over large wavelengths ranges (figure 14), and added imaging optics at the entrance to the spectrograph to better match the f/7.0 instrument to the f/2.3 optical fibers. The end result was an approximately 2.3x increase in collection efficiency over the previous run. We also reduced the focal spot of the fiber from 1.6mm to 1.0mm or 2.6x (to gain better spatial resolution). The relative intensities on the streak camera for the two data sets were comparable. Figure 13 shows the focusing optics.

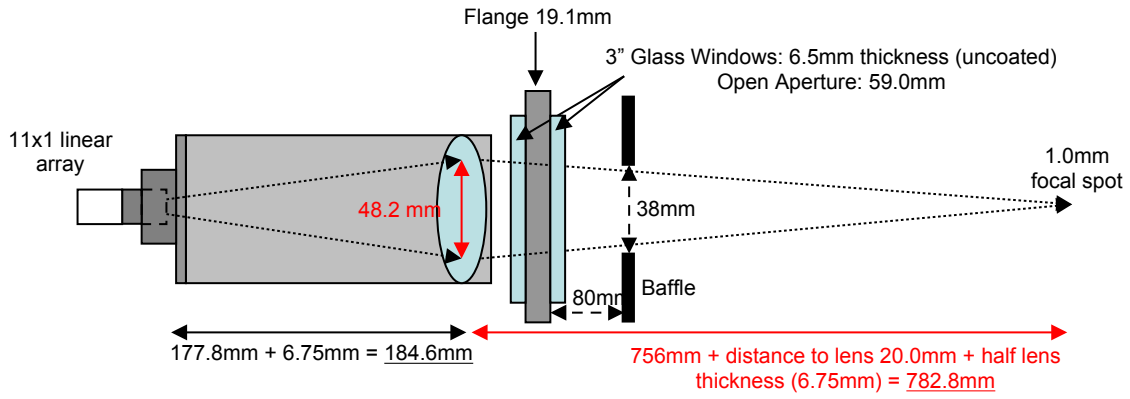

Figure 13. Focusing optics for SMP diode shots 762-767.

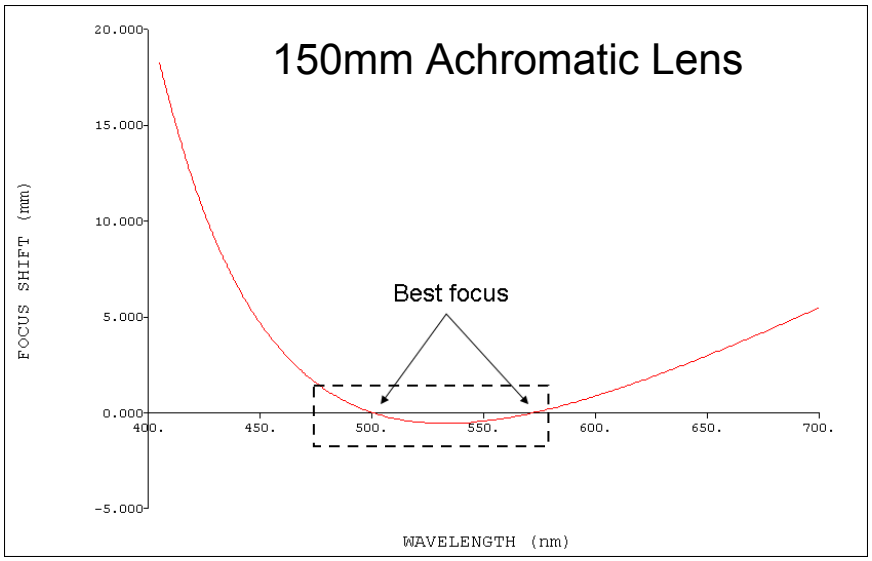

Figure 14. Focus versus wavelength for SMP shots 762-767 (compare to figure 5).

6. Experimental Results: (Shots 762-767)

This new data set consisted of six shots, three taken on-axis (762, 764, and 765) and three taken 7.5mm off-axis (763, 766, and 767). In addition to the 7.5 mm off-axis position, we added a 4.0 mm off-axis shot (767) in hopes of obtaining better information regarding the radial variation of the spectra in time.

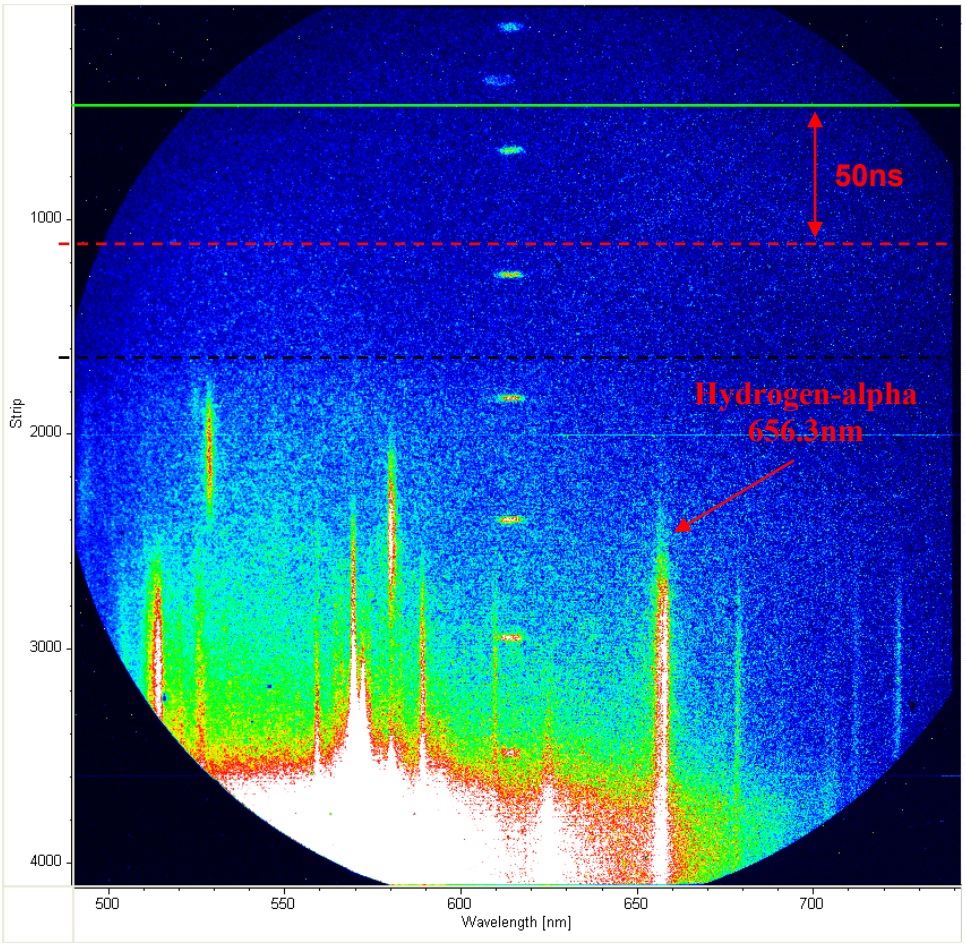

Figure 15. Off-axis spectra (shot 766).

Four of the shots spanned the wavelength region from 4000Å to 6500Å and the last two shots looked further into the red (5000Å to 7300Å) to measure the H-alpha spectra.

For these shots, a lot of emphasis was placed on looking at the aluminum and carbon lines, as these species had been observed in the previous experiments. In particular, the Al III lines at 4480Å, 4512Å, and 4529Å, and at 5696Å and 5723Å. Since this spectra had better collection

optics, we were able to distinguish line emission off-axis relatively early in time with little background continuum (figure 15). We observed several higher charge state lines, C IV 4658Å and C IV 5801Å, in addition to oxygen and/or silicon contaminant lines, indicating higher electron temperatures early in time. Since, the charge states are low (up to plus three), the electron temperatures are still in the few eV range, justifying the earlier analyses. Hydrogen neutral lines were observed 60ns after the end of the pulse off-axis in shot 766 (figure 15). Hydrogen was not measured on-axis, but it is expected that the high electron densities observed on-axis, would results in significant broadening of the Balmer alpha line, making its identification above the continuum difficult [25].

All of the 7.5 mm off-axis spectra, plus the 4.0 mm off-axis spectra, begin after the radiation pulse, while the on-axis spectra starts during the peak of the radiation pulse (indicating a small, millimeter-sized, spatial extent for the plasma during the pulse). The on-axis spectra are continuum emissions while the off-axis spectra are line emissions. Very late in time the 7.5 mm off-axis spectra shows increased continuum emission and some line broadening indicative of densities in the 10^17 cm^{-3} range (less than the 10^18 cm^{-3} range from the previous run in spite of no significant differences between the shots). The 4.0 mm off-axis shot (767) was particularly interesting (see figure 16). It doesn't give measureable spectra until after the radiation pulse, and begins with line emission and low continua; the continua quickly increase in time along with broadening and merging of the Al III 5696Å and 5723Å lines (figure 17). The Al III line broadening clearly shows the increasing electron density occurring in the diode. To have such broadening of these Al III lines, densities increasing into the 10^18 cm^{-3} range are required [26]. Spectral calculations show an order of magnitude increase in density from mid 10^17 cm^{-3} to 6x10^18 cm^{-3} during a span of ~60 ns from 120-180 ns after the start of the current pulse. Note that these densities are greater than those measured in shot 412 at 7.5 mm, which is consistent with a decreasing radial density profile. The boundary between the early-time line emission and start of the rise in the continuum is indicative of a low density plasma shell surrounding a higher density core early in time (figure 8).

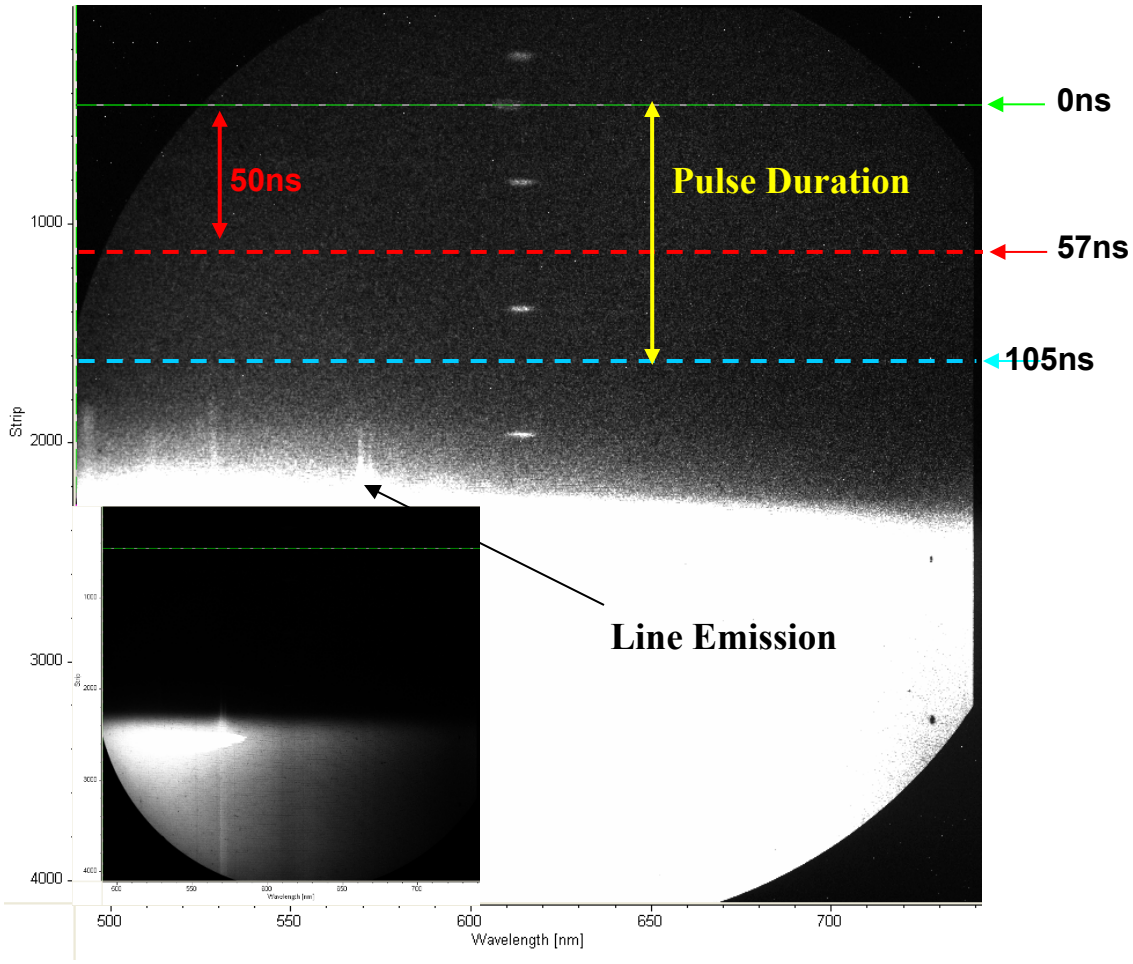

Figure 16. 4.0mm off-axis streaked spectra (shot 767).

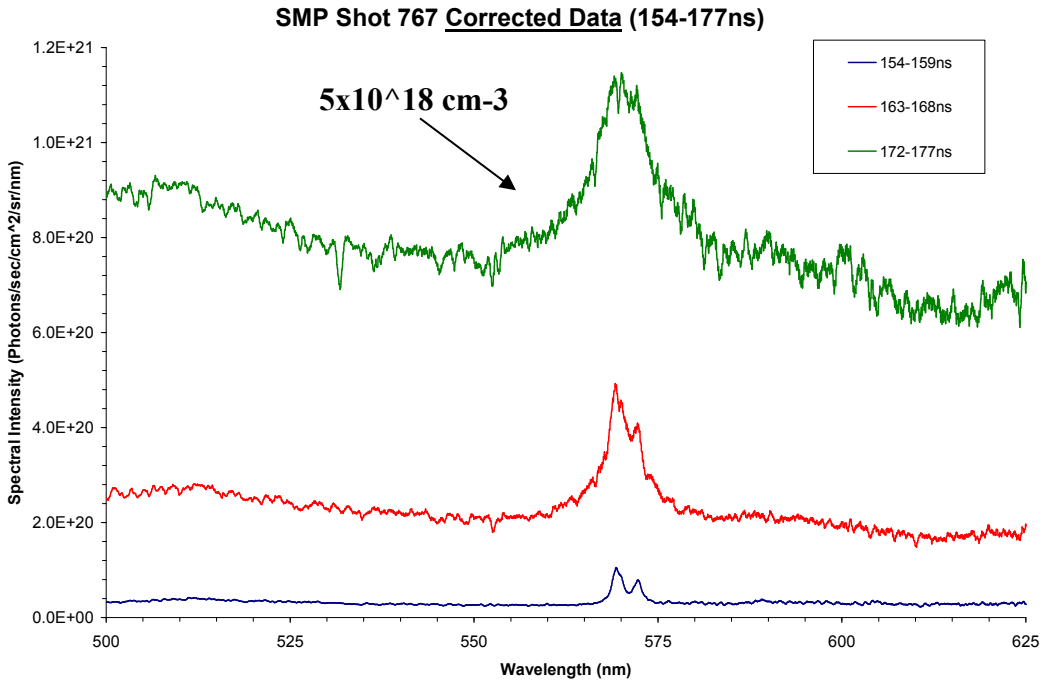

Figure 17. Al III 5696A and 5723A emission spectra (shot 767).

In contrast, the on-axis spectra shows strong continuum emission during the pulse-time, increasing in intensity by a factor of 36x in 25 ns, which is the equivalent to an increase in density of 6x (figure 18). Since it is assumed that the plasma is originating from the anode surface where the beam is focused, the differences in arrival times of the plasma off-axis lead to the conclusion that during the pulse, the spatial extent of the plasma is small (a few millimeters). While plasma does occur over large radii (centimeter) early in time prior to the electron beam pinching, these plasmas are less dense and do not contribute significantly to the continua measured above. Additional experiments at smaller radii are planned to better quantify the plasma size early in time.

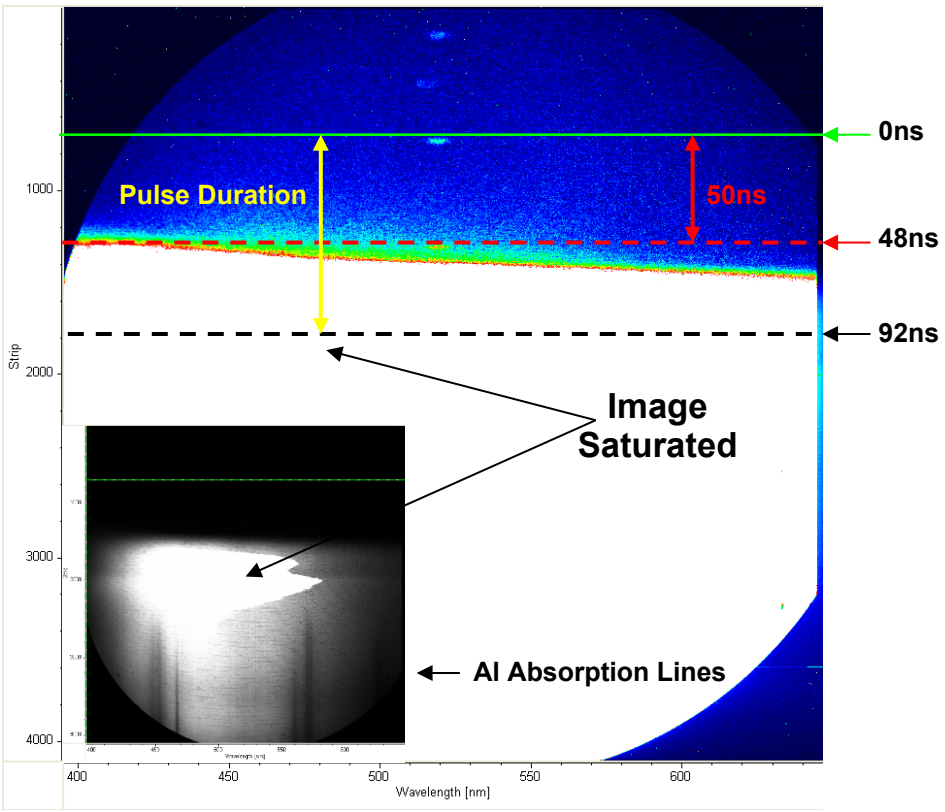

Figure 18. On-axis streaked spectra (shot 764).

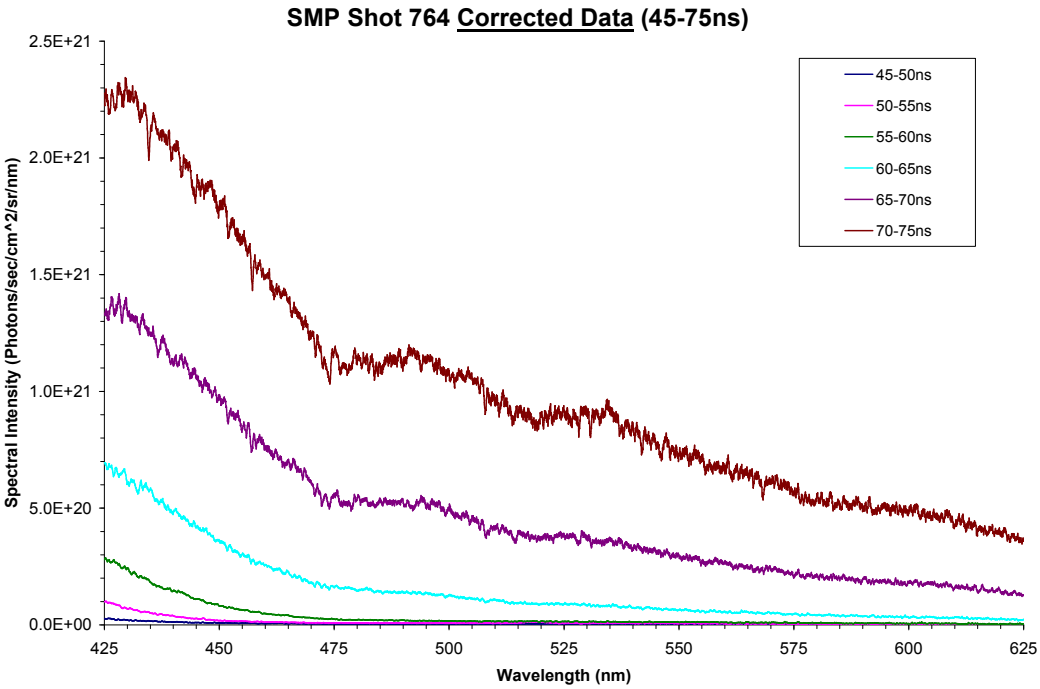

Figure 19. Continuum emission versus time (shot 764).

Plasmas are also observed on the cathode. Since these plasmas form on the outer regions of the cathode surface (hollow-cathode), emission light from cathode plasmas becomes increasingly important as spectra are collected across the A-K gap towards the cathode. We observe light emission from the cathode on gated images (figure 20), silicon PIN photodiodes (figures 3 and 4), and with streak cameras (figure 21), during the time of the radiation pulse. Near the cathode, the plasma is likely hollow, and light from this hollow, cathode plasma is collected along a line of sight which includes any on-axis contributions from the anode plasma. Since the cathode itself is hollow, it is possible for the on-axis anode plasma to expand into the hollowed region of the cathode, and not short the diode until it makes contact the back wall (see figure 22). Since the depth of this hollowed region is 27.5 mm, or over twice the A-K gap distance, it is reasonable to assume that this hole allows the diode to continue operating, even while high density plasmas are present in the A-K gap (see figure 22).

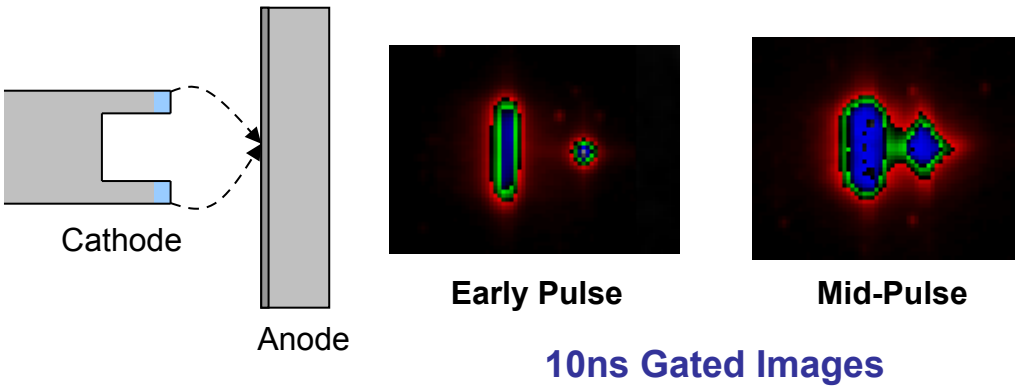

Figure 20. Optical gated images of plasma formation in SMP diode.

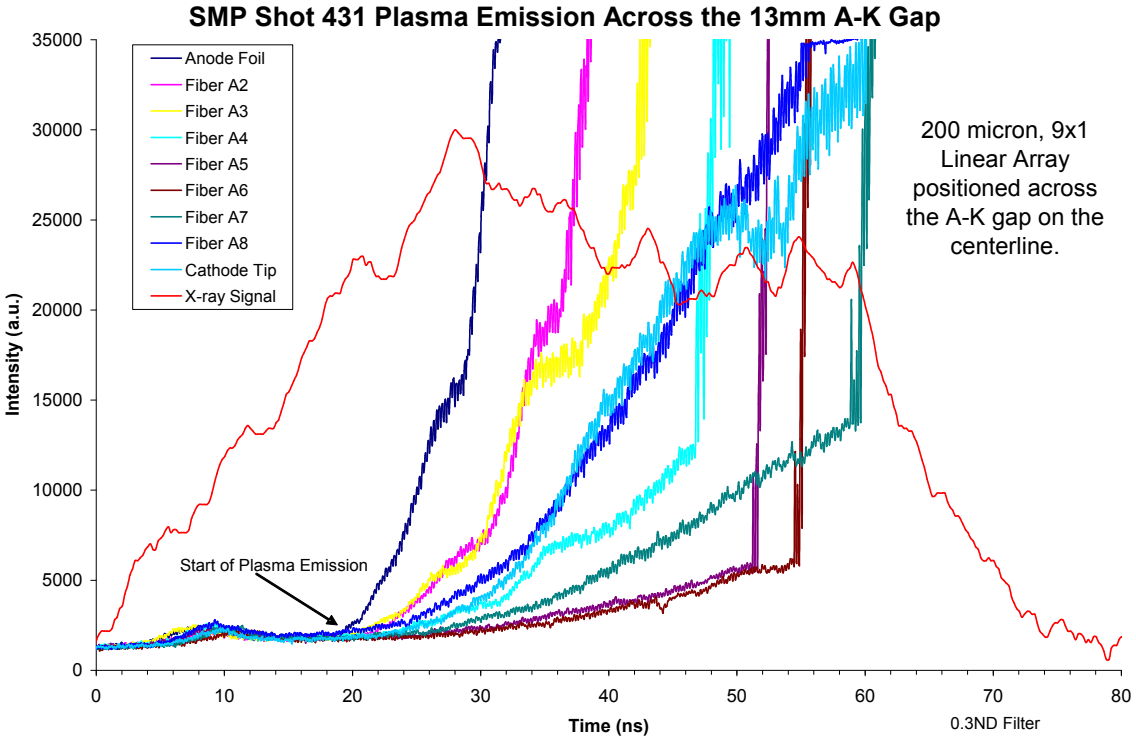

Figure 21. Plasma light emission across A-K gap during radiation pulse (direct fiber input into streak camera).

Furthermore, this predicts that a solid cathode (or a hollow one with less depth) would short out sooner, which can be tested experimentally. The hollow-cathode with a shorter depth is attractive experimentally, since the electron emission area and beam focusing mechanism would essentially remain the same.

7. LSP Simulations and Future Work

While much simulation work has been done on this diode in Lsp [9] (figure 22), a lot of the input parameters, including plasma generation and contaminant monolayers, are subjective. The simulations need experimental input parameters. When disagreements exist between the experiments and simulations, it is important to explore these differences and attempt to explain them. To date, the simulations model cathode and anode plasmas and suggest methods for the impedance behavior of the diode. Much

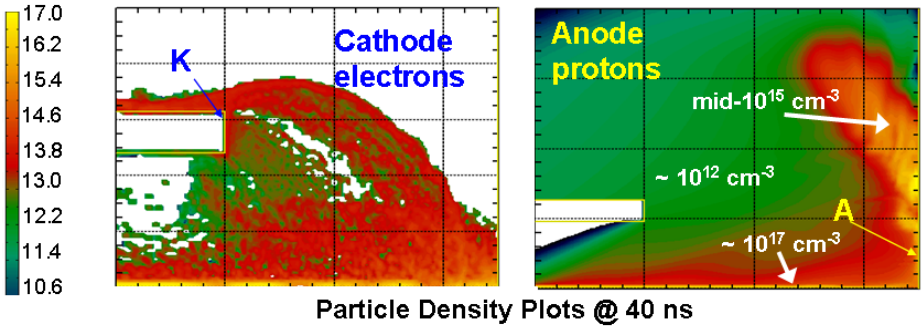

Figure 22. LSP simulations of cathode electrons and anode protons for the SMP diode.

of the recent focus has been on cathode plasmas, although anode plasmas of reasonably high densities (10^{15} - 10^{17} cm^{-3}) have been observed both on and off-axis in these simulations [9] (figure 22). Plans are underway to try and better understand these differences and design experiments around answering specific questions which either support or refute various simulation models. In the end, we need a good physics understanding of how this diode works to allow for continued improvements to be made, ultimately resulting in a better radiographic source.

8. REFERENCES

1. D. Johnson, V. Bailey, R. Altes, P. Corcoran**,** *et al*., "Status of the 10MV, 120kA RITS-6 Inductive Voltage Adder," Proceedings of the 15th IEEE International Pulsed Power Conference, 314 (2007).

2. K. Hahn, N. Bruner, M.D. Johnston, B.V. Oliver, *et al*., "Overview of the Self-Magnetic Pinch Diode Investigations on RITS-6," IEEE Trans. on Plasma Science, 38, 2652 (2010).

3. B.V. Oliver, K. Hahn, M.D. Johnston, and S. Portillo, "Advances in High Intensity e-Beam Diode Development for Flash X-ray Radiography," Acta Physica Polonica A, 115, 1044 (2009).

4. M.D. Johnston, K. Hahn, D. Rovang, S. Portillo, *et al*., "Plasma Spectroscopy Diagnostics in Pulsed-Power X-ray Radiographic Diode Research," Proceedings of the 14th IEEE International Pulsed Power Conf., 1129 (2005).

5. E. Stambulchik and Y. Maron, "A Study of Ion-Dynamics and Correlation Effects for Spectral Line Broadening in Plasma: K-shell Lines," Journal of Quantitative Spectroscopy & Radiative Transfer, 99, 730 (2006).

6. E. Stambulchik and Y. Maron, "Stark Effect in High-n Hydrogen-like Transitions," Journal of Physics B. 41, 095703 (2008).

7. Yuri V. Ralchenko and Y. Maron, "Accelerated Recombination Due to Resonant Deexcitation of Metastable States," Journal of Quantitative Spectrscopy & Radiative Transfer, 71, 609 (2001).

8. LSP is a licensed product of ATK Mission Research, Albuquerque, NM 87110.

9. D.R. Welch, D.V. Rose, N. Bruner, R.E. Clark, *et al*., "Hybrid Simulation of Electrode Plasmas in High-Power Diodes," Phys. of Plasmas, 16, 123102-1 (2009).

10. A.D.J. Critchley, A.D. Heathcote, and M.D. Johnston, "Electrode Plasmas During Self-Magnetic-Pinch E-Beam Diode Operation," IEEE Trans. on Plasma Science, 36, 1214 (2008).

11. A.E. Blaugrund and G. Cooperstein, "Intense Focusing of Relativistic Electrons by Collapsing Hollow Beams," Phys. Rev. Letters, 34, 461 (1975).

12. S.B. Swanekamp, G. Cooperstein, J.W. Schumer, D. Mosher, *et al*., "Evaluation of Self-Magnetically Pinched Diodes up to 10MV as High-Resolution Flash X-ray Sources," IEEE Trans. on Plasma Science, 32, 2004 (2004).

13. D.D. Hinshelwood, G. Cooperstein, D. Mosher, D.M. Ponce, *et al*., "Characterization of a Self-Magnetic-Pinched Diode," IEEE Trans. on Plasma Science, 33, 696 (2005).

14. D.D. Hinshelwood, R.J. Allen, R.J. Commisso, G. Cooperstein, *et al*., "High-Power Self-Pinch Diode Experiments for Radiographic Applications," IEEE Trans. on Plasma Science, 35, 565 (2007).

15. A.E. Blaugrund, G. Cooperstein, "Relativistic Electron Beam Pinch Formation Processes in Low Impedance Diodes," Phys. of Fluids, 20, 1185 (1977).

16. J.E. Maenchen, G. Cooperstein, J. O'Malley, and I. Smith, "Advances in Pulsed Power-Driven Radiography Systems," Proc. IEEE, 92, 1021, (2004).

17. M.E. Cuneo, "The Effect of Electrode Contamination, Cleaning, and Conditioning on High-Energy, Pulsed Power Device Performance," IEEE Trans. Dielectric Electrical Insulation, 6, 469 (1999).

18. McPherson, Inc., 7A Stuart Road, Chelmsford, MA 01824.

19. National Security Technologies, LLC., Livermore Operations, 161 South Vasco Road, Suite A, Livermore, CA 94550.

20. R.W. Olsen, "EG&G, Inc., Fast Streak Camera Operation," SPIE-High Speed Photography, Videography, and Photonics VI, 981, 71 (1988).

21. Polymicro Technologies, LLC, 18019 North 25th Ave., Phoenix, AZ 85023.

22. M.D. Johnston, B.V. Oliver, D.W. Droemer, B. Frogget, *et al*., "Absolute Calibration Method for Nanosecond-Resolved, Time-Streaked, Fiber Optic Light Collection, Spectroscopy Systems," SAND Report, 2010-2470, (2010).

23. M.D. Johnston, B.V. Oliver, S. Portillo, T.A. Mehlhorn, *et al*., "Investigation of Plasma Formation and Propagation in Relativistic Electron Beam Diodes," 35th IEEE International Conference on Plasma Science, Karlsruhe, Germany, (2008).

24. H.R. Griem, Plasma Spectroscopy, McGraw-Hill Book Inc., New York (1964).

25. St. Böddeker, S. Gunter, A. Konies, L. Hitzschke, *et al*., "Shift and Width of the H_α Line of Hydrogen in Dense Plasmas," Physical Review E, 47, 2785 (1993).

26. L.Y. Chan, A.N. Mostovych and K.J. Kearney, "Stark Broadening Measurements of Al(III) Doublet Lines in Dense and Optically-Thin Laser Plasmas," Journal of Quantitative Spectroscopy and Radiative Transfer, 55, 815 (1996).

27. Roth, A., Vacuum Technology, North-Holland, Amsterdam (1990).

28. O'Hanlon, J. F., A User's Guide to Vacuum Technology, John Wiley & Sons, New York (1989).

29. Hayward, D.O. and Trapnell, B.M., Chemisorption, Butterworths, London (1964).

30. Li, H., Belkind, A., Jansen, F., and Orban, Z., "An in Situ XPS Study of Oxygen Plasma Cleaning of Aluminum Surfaces," Surface and Coatings Technology, 92, 171 (1997).

31. Belkind, A., Krommenhoek, S., Li, H., *et al*., "Removal of Oil from Metals by Plasma Techniques," Surface and Coatings Technology, 68/69, 804 (1994).

32. Kersten, H., Steffen, H., Behnke, J.F., "Investigations on Plasma-Assisted Surface Cleaning of Aluminum Contaminated with Lubricants," Surface and Coatings Technology, 86/87, 762 (1996).

33. Cuneo, M.E., Menge, P.R., Hanson, D.L., Fowler, W.E., *et al*., "Results of Vacuum Cleaning Techniques on the Performance of LiF Field-Threshold Ion Sources on Extraction Applied-B Ion Diodes at 1-10 TW," IEEE Transactions on Plasma Science, 25, 229 (1997).

34. Schreiber, J., Kaluza, M., Gruner, F., Schramm, U. *et al*., "Source-size Measurements and Charge Distributions of Ions Accelerated from Thin Foils Irradiated by High-Intensity Laser Pulses," Applied Physics B, 79, 1041 (2004).

35. Gilgenbach, R.M., Hochman, J.M., Jaynes, R.L, Cohen, W.E., *et al*., "Optical Spectroscopy of Plasma in High Power Microwave Pulse Shortening Experiments Driven by a μs E-Beam," IEEE Transactions on Plasma Science, 26, 282 (1998).

36. Cohen, W.E., Gilgenbach, R.M., Jaynes, R.L., Peters, C.W., *et al*., "Radio-frequency Plasma Cleaning for Mitigation of High-Power Microwave-pulse Shortening in a Coaxial Gyrotron," Applied Physics Letters, 77, 3725 (2000).

37. Menge, P.R. and Cuneo, M.E., "Quatitative Cleaning Characterization of a Lithium-Fluoride Ion Diode," IEEE Transactions on Plasma Science, 25, 252 (1997).

38. Vermare, C., Davis H.A., Moir, D.C., and Hughes, T.P., "Ion Emission from Solid Surfaces Induced by Intense Electron Beam Impact," Physics of Plasmas, 10, 277 (2003).

Appendix A: Surface Contaminants

A lot of information is available regarding high vacuum systems and surface contaminants on metals. Many studies have been made over the years and most of this information is available in several texts and articles [27-36]. Most of these publications deal with the properties of gases and metal surfaces and includes discussions of vapor pressures, evaporation/condensation rates, sticking coefficients, etc. In addition, many measurements have been made of gas permeation into metals (ex. low for aluminum due to the oxide coating).

There are several things to consider regarding surface contaminants on diode components on RITS. First we need to consider the composition of the components, since different materials absorb and adsorb species by different mechanisms and in different amounts. For the aluminum foil anode, we know there is a certain amount of contamination present prior to it being placed in the vacuum chamber. This includes an oxide layer (~40-100 Angstroms thick) along with hydrocarbon contaminants from the manufacturing process (similar techniques to fine wires production) (~100-500 Angstroms thick). In addition, when inside the RITS vacuum chamber, at 10^{-5} Torr vacuum, we can expect many monolayers of water vapor (typically 10-20), where each monolayer contains ~10^{15} particles per cm^2. The primary contaminant species are hydrogen, carbon, and oxygen, found in various hydrocarbons, organic compounds (CO and CO_2 for example), and water vapor. In addition, we use an insulating solution composed of various volatile hydrocarbons (toluene, ethyl acetate, and hexane) combined with a silicone based diffusion pump oil which add to the surface contaminants. In total, it is not unlikely to expect 100's of monolayers of material on top of the base aluminum, with a large fraction of these contaminants being hydrogen (~50-70%). Only a small amount of hydrogen gas is expected to diffuse through the aluminum itself (not the case for other diode materials such as tantalum), still the surface hydrogen inventories alone are great enough to account for 10^{18} cm^{-3} plasmas seen in the SMP diode. Since we know, that high temperatures >100C over long periods are required to remove these types of contaminants from the system, we can only assume that they are present during the RITS shots.

Peter Menge's IEEE Article on LiF ion diode [37]: Shows that dozens of monolayers of contaminants exist on 1 micron thick LiF coatings on stainless steel substrates. Measurements were done at $2x10^{-5}$ Torr vacuums. Typically there are 13-45 monolayers (up to 200 Angstroms depth) of carbon impurities on the surface after 24 hr. in a 10^{-5} Torr vacuum, and about 5 monolayers of oxygen. Also, there are about 10 equivalent monolayers in contact with the surface every second. The article discusses RF cleaning regimes, and shows that about 10 monolayers of carbon will return within ten minutes from a cleaned surface.

Christophe Vermare's POP Article on DARHT foil experiments [38]: The experiments performed on DARHT and the supporting PIC simulations due not preclude proton plasmas as being responsible for the development of observed beam instabilities. The conclusion of heavier ions being present was based on calculations which showed that ~40 monolayers of water vapor would be required to produce a SCL proton beam under DARHT conditions (3 mm beam at 20 MeV for 30 ns), while only one monolayer of heavier ions (H_2O+, OH+, and O+) would be required. They also measured beam oscillations experimentally at 125 MHz which compared well with H+ oscillations in LSP at 140 MHz (higher mass species would have lower frequency oscillations), leading to the authors conclusion that, "this provides evidence for the presence of a significant number of H+ ions, produced by ionization of desorbed water in the experiments."

Insulating Oil Solution:
2 Parts Silicon-based Diffusion Pump Oil (CMP-702)
1 Part Organic Solvent Mixture:

55%	($C_6H_5CH_3$)	Toluene (Methylbenzene)
35%	($CH_3CO_2CH_2CH_3$)	Ethyl Acetate
10%	($CH_3(CH_2)_4CH_3$)	Hexane

Colloidal Silver Solution used on SMP Cathode:

Silver	59-61%
Isopropyl Alcohol	20-35%
Methyl Ethyl Ketone	10-15 %
Ethyl Acetate	2-10%

DISTRIBUTION

2	Voss Scientific Attn: D. R. Welch 418 Washington St. SE Albuquerque, NM 87108		
1	Dept. of Electrical & Computer Engineering Attn: Edl Schamiloglu MSC01 1100 1 University of New Mexico Albuquerque, NM 87131-001		
5	MS1168	M. D. Johnston	1656
3	MS1168	B. V. Oliver	1656
1	MS1168	T. J. Webb	1656
1	MS1168	J. J. Leckbee	1656
1	MS1193	D. W. Droemer	16561
1	MS1193	M. D. Crain	16561
1	MS1193	M. E. Cuneo	1643
1	MS1193	D. C. Rovang	1643
1	MS1196	K. D. Hahn	1677
1	MS1196	R. J. Leeper	1677
1	MS1196	J. E. Bailey	1677
1	MS0899	Technical Library	9536 (electronic copy)


Sandia National Laboratories